



DEM Investigation of Borehole Deformation and Stress Induced Fracture Geometry in Coal

Huang Shan^{1,2} · Lu Yiyu^{1,2} · Ge Zhaolong^{1,2} · Yunzhong Jia^{1,2}  · Zhou Zhe^{1,2} · Lu Changzheng^{1,2}

Received: 28 January 2024 / Accepted: 26 June 2024

© The Author(s), under exclusive licence to Springer-Verlag GmbH Austria, part of Springer Nature 2024

Abstract

To prevent economic losses caused by borehole breakout during coalbed methane extraction, it is essential to understand the mechanisms of borehole deformation and the distribution patterns of stress-induced fractures. However, previous research efforts have failed to address these aspects adequately. This article investigates the geometry nature of borehole breakout in pre-loaded coal samples under various factors using the discrete element method (DEM). The results revealed significant distinctions in borehole breakout behaviour between coal and other geological materials. In the case of coal, the geometry of breakout is particularly pronounced during the initial stages of failure. However, as stress differentials intensify, the geometry undergoes relatively minimal alterations compared to other rock formations, suggesting a relatively weak sensitivity. The geometry of the borehole breakout in the coal seam widened and deepened as the stress difference increased and the coal elastic modulus decreased. The breakout volume first increased significantly and remained stable as the stress difference increased. A critical threshold line is proposed to represent the macroscopic failure of coal rock caused by drilling, considering the combined effects of elastic modulus and stress differential. The region below the threshold line represents the trend of macroscopic failure after drilling instability, while the region above the threshold line indicates a stable trend. The findings of this study have practical implications for engineering applications.

Highlights

- Various factors (stress difference, borehole size, coal elastic modulus) influence the geometry nature of borehole breakout in coal.
- Breakout depth and breakout width in simulated coal rock show a linear positive correlation with stress differences.
- Borehole deformation in coal seams is apparent once it occurs but shows lower sensitivity to the in-situ stress difference compared to sandstone and limestone.
- A decisive criterion for determining whether borehole breakout leads to macroscopic fracture in coal rock is suggested by considering the joint impact of elastic modulus and stress difference.

Keywords Borehole deformation · Borehole breakout geometry · Discrete element method (DEM)

1 Introduction

Borehole breakout is the distortion and deformation to the borehole's surroundings caused by the redistribution of in-situ stress due to drilling, which leads to different types of borehole breakout in geo-materials, including V-shaped or slot-shaped breakout along the minimum horizontal stress direction, spiral-shaped breakout, and others (Fig. 1). If left unaddressed, these localized stress concentrations can result in fractures, deformation, and failure, such as borehole collapse, washout, and completion difficulties,

✉ Yunzhong Jia
yunzhong.jia@cqu.edu.cn

¹ State Key Laboratory of Coal Mine Disaster Dynamics and Control, Chongqing University, Chongqing 400044, China

² School of Resources and Safety Engineering, Chongqing University, Chongqing 400044, China

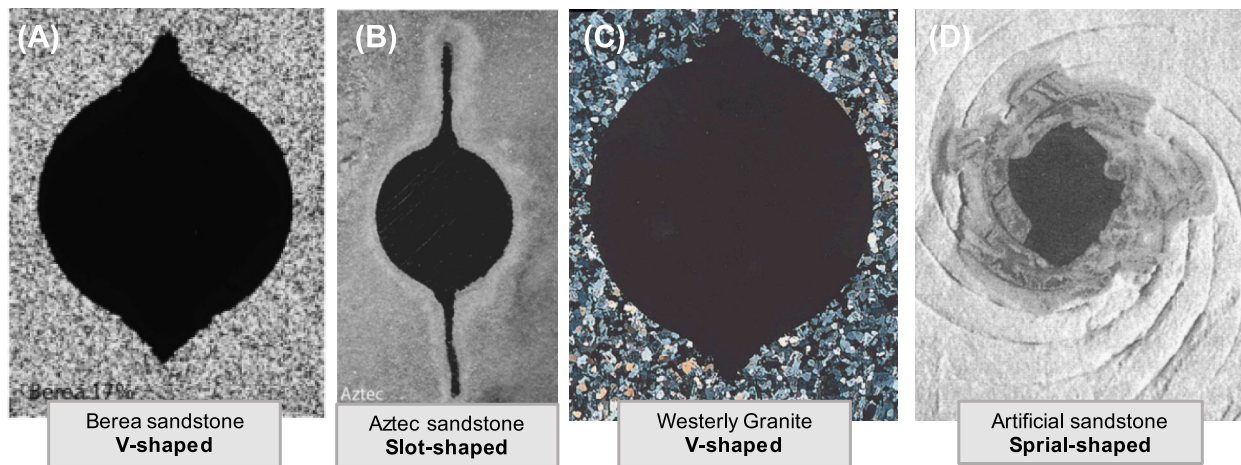


Fig. 1 Illustration of several borehole breakout phenomena: **A**, Berea sandstone showing V-shaped breakout (Haimson 2007); **B**, Aztec sandstone showing slot-shaped breakout geometry; **C**, Westerly Gran-

ite showing V-shaped breakout geometry (Song 34); **D**, Spiral-shaped geometry observed in an artificial sandstone under the same stress in both directions (Van den Hoek PJ 17)

ultimately leading to economic losses and impacting coalbed methane extraction efficiency (Zoback et al 40; Cheatham 5; Haimson and Lee 14; Marschall et al 25; Jianping et al 20). However, its occurrence mechanism, crack propagation and distribution patterns have been rarely addressed in previous studies.

Cheng (Fushan et al 12) reported that in the DaNiuDi gas field in the northern part of the Ordos Basin, 50% of the coal bed drilling operations have resulted in borehole instability accidents. Five wells, including DP3, DP16, and DP18, collapsed severely, leading to side-drilling backfilling, while DP7 encountered blockages and had to be prematurely completed, resulting in significant economic losses. In a study by Shen (Ruichen 28), borehole instability data from various basins in China were surveyed. The findings revealed that the Tuha, Tarim, and Ordos basins, as well as Shanxi Province, are the regions most significantly affected by wall stability issues during coal bed drilling operations. Ai (Ai et al 1) found that coal bed cleats expanded after being soaked in borehole water for two days, destabilising previously stable wellbores, which provides evidence of a hysteresis effect in the instability of coal bed drilling. He (He et al 16) established the functional relationship between effective radial and tangential shear and in-situ stresses and pore pressure of borehole instability locations through on-site monitoring. Many scholars have qualitatively observed the phenomenon of drilling-induced fractures in coal seams through field and laboratory experiments. However, there has been little quantitative research on the instability mechanisms and factors affecting fracture geometry. Additionally, the influence mechanism of coal strength on borehole deformation and

instability remains unclear due to the intrinsic discreteness of coal as a geological material.

Although analytical solutions exist (Zoback et al 40; Barton et al 4; Wang et al 36; Xiang et al 37) for the near-wellbore stress distribution in geo-materials, the dynamic process of stress redistribution following fracture creation makes modelling the failure evolution challenging using constitutive methods. Additionally, it is challenging to conduct experiments on the development of borehole breakout geometry in coal rock, both in the field and indoors, due to limitations in observation methods. To address this issue, a micromechanics-based approach, such as the Discrete Element Method (DEM), may aid in comprehending the physical process and underlying mechanisms of borehole breakouts under varying borehole sizes, in situ stresses, etc. The discrete element method (DEM) (Cundall 7; Fakhimi et al 11; Potyondy and Cundall 26; Hazzard et al 15) is employed to study the geometry of borehole breakouts in coal rock under various conditions. A detailed examination of the failure process and underlying mechanisms of V-shaped borehole breakouts is presented in this paper. To begin with, a brief introduction of the simulation methodology is provided, followed by careful calibration of microscopic parameters used in the simulation through laboratory tests and analytical methods. Subsequently, breakout geometries are investigated under varying stress differences, borehole sizes, and intrinsic properties of coal rock. Furthermore, the numerical simulation results of coal drilling-induced fractures are compared with those of other rocks. Finally, the practical implications of the findings for field applications are

discussed. This study contributes to a better understanding of borehole breakouts in coal rock and provides insights for optimising drilling operations.

2 Numerical Simulation Methodology

2.1 Bonded Parallel Model (BPM)

The Discrete Element Method (DEM) eliminates the macroscopic continuity assumption inherent in traditional continuum mechanics models by amalgamating particles into macroscopic materials. Consequently, DEM proves to be a fitting approach for simulating nonlinear rock material behaviors such as substantial deformation and cracking. At the grain scale, microfractures occur and propagate within rocks. A commonly held belief is that a 2D particle assembly based on the Bonded Parallel Model (BPM) accurately represents actual rock samples, with spherical particles cemented at contacts via finite disks termed “bonds” (Song et al Itasca 19). The BPM can effectively reflect the mechanical properties of rock materials by simultaneously transmitting force and moment. It uses the force–displacement law and Newton’s law of motion in alternating calculation iterations. The force–displacement law updates the contact force of the effective contact area, while the law of motion updates the particle–particle

and particle–boundary position, ultimately achieving a new equilibrium. Fish language is utilized for data processing to write the function, and DEM records interparticle adhesion destruction, crack distribution and number, contact force field, and other information. This report implements DEM simulation using commercial software PFC2D. For more details on the BPM model, readers can refer to the previous research articles (Potyondy and Cundall 26; Hazzard et al 15; Itasca 19; Song et al 30; Xu et al 38; Bai et al 2; Lu et al 24).

2.2 Parameter Calibration

PFC functions with input parameters that differ from the mechanical parameters obtained through macro-scale physical tests, such as Young’s modulus, Poisson’s ratio, and UCS. Hence, achieving accurate PFC modelling requires calibration of input microscale parameters, which can be a time-consuming and laborious trial-and-error process, greatly reliant on physical test results. In this article, a uniaxial compression test was conducted using the Precision Material Testing Machine (AG-250kN-IS) at the State Key Laboratory of Coal Mine Disaster Dynamics and Control, Chongqing University, on coal rock samples. Subsequently, by performing multiple numerical simulations of the uniaxial compression test using PFC, the numerically modelled uniaxial compressive strength (UCS) values, tensile

Table 1 Calibrated micro-mechanical parameters and other properties of the numerical specimen

Micro-mechanical parameters			Value
Ball-ball contact Young’s modulus, \bar{E} (GPa)			1.48
Parallel-bond Young’s modulus, E (GPa)			1.48
Parallel-bond tension strength, $\bar{\sigma}_t$ (MPa)			13.1
Parallel-bond cohesion, c (MPa)			27.2
Parallel-bond normal-to-shear stiffness ratio, \bar{k}_n/\bar{k}_s (-)			2.8
Internal friction angle, ϕ (°)			21
Friction coefficient, η (-)			0.1
Macro-mechanical parameters		Experimental value	Calibrated value
UCS, σ_c (MPa)		26.24	26.95
TS, σ_t (MPa)		1.54	1.57
Poisson’s ratio, ν (-)		0.38	0.42
Elastic Modulus, E_c (GPa)		1.97	1.99
Model’s other properties		Radius of wellbore (m)	Ball maximum radius (m)
		$1.8 \sim 2.2 \times 10^{-2}$	6.6×10^{-4}
Ball density (kg/m ³)		Model length & height (m)	Ball-facet contact amounts in intact sample (-)
1550	0.5		Ball-ball contact amounts in intact sample (-)
			83,415

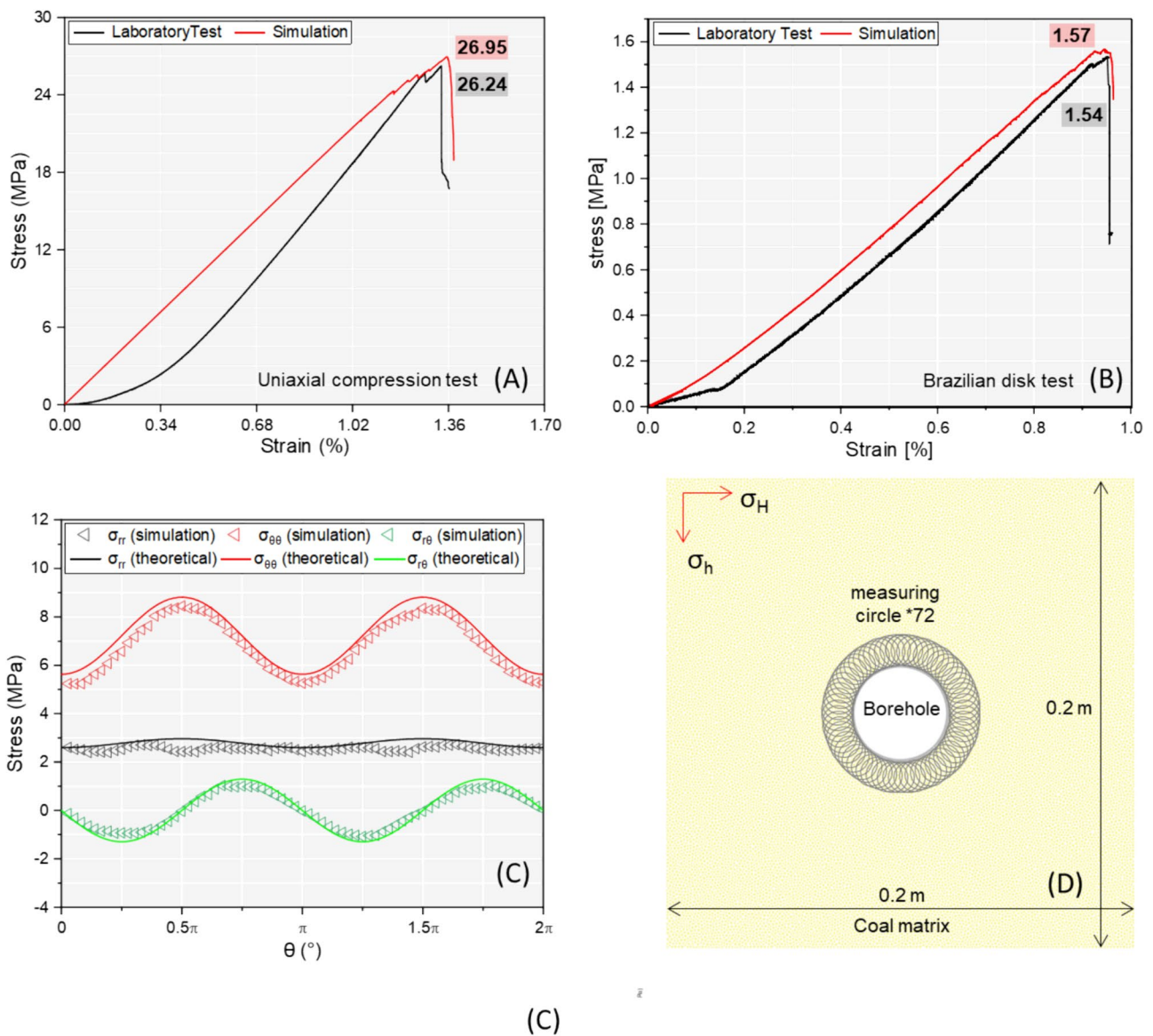


Fig. 2 a-b, comparison of stress–strain curves: uniaxial compression test and brazilian tension test (The peak values of each curve are marked with corresponding colors); **c**, comparison of stress around

borehole from simulation and theoretical calculation; **d**, illustration of sample set-up and arrangement of 72 measuring circles used during calibration procedure

strength (TS), Poisson’s ratio, elastic modulus were optimized to reflect the actual experimental results (Table 1). The stress–strain curve obtained is presented in Fig. 2A. Further details on this step can be found in our previous study (Lu et al 24).

As this paper simulates the unstable fracturing behaviour of coal rock after drilling, the key point that validates this model is the calibration of stress distribution around the

circular borehole, in addition to the correction of macro-scale strength parameters. The state of stress in this scenario can be described using the Kirsch equations, which are commonly applied to a hole in an infinite plate. Fairhurst (Fairhurst 10) adapted these equations for plane strain conditions and drilling a hole in a pre-stressed geo-material. Haimson (Haimson 13) further updated the equations to incorporate the influence of borehole and pore fluid pressures:

$$\sigma_{rr} = \frac{1}{2}(\sigma_H^* + \sigma_h^*) \left(1 - \frac{a^2}{r^2}\right) + \frac{1}{2}(\sigma_H^* - \sigma_h^*) \left(1 - 4\frac{a^2}{r^2} + 3\frac{a^4}{r^4}\right) \cos 2\theta + \frac{\Delta P a^2}{r^2}$$

$$\sigma_{\theta\theta} = \frac{1}{2}(\sigma_H^* + \sigma_h^*) \left(1 + \frac{a^2}{r^2}\right) - \frac{1}{2}(\sigma_H^* - \sigma_h^*) \left(1 + 3\frac{a^4}{r^4}\right) \cos 2\theta - \frac{\Delta P a^2}{r^2}$$

$$\sigma_{r\theta} = -\frac{1}{2}(\sigma_H^* + \sigma_h^*) \left(1 + \frac{2a^2}{r^2} - 3\frac{a^4}{r^4}\right) \sin 2\theta \quad (3)$$

where, σ_{rr} is the radius stress, $\sigma_{\theta\theta}$ is the tangential stress, $\sigma_{r\theta}$ is the shear stress acting around the borehole wall. a is the borehole radius, r is the distance of the measuring point to the borehole centre. θ denotes the angular direction measured counterclockwise from the direction of σ_H . ΔP is the difference between the fluid pressure in the borehole and the formation. Since pore water pressure is ignored in this study, $\Delta P = 0$. The DEM model in this section incorporates a set of 72 measurement circles (Itasca 19), each with a diameter of 1 cm, to determine the stress state, as illustrated in Fig. 2C. The resulting stress measurements can be converted to polar coordinates using the equations presented by previous studies (Sokolnikoff and Specht 29; Duan and Kwok 9):

$$\sigma_{rr} = \sigma_x \cos^2 \theta + \sigma_y \sin^2 \theta + 2\tau_{xy} \sin \theta \cos \theta \quad (4)$$

$$\sigma_{\theta\theta} = \sigma_x \sin^2 \theta + \sigma_y \cos^2 \theta - 2\tau_{xy} \sin \theta \cos \theta \quad (5)$$

$$\tau_{r\theta} = (\sigma_y - \sigma_x) \sin \theta \cos \theta + \tau_{xy} (\cos^2 \theta - \sin^2 \theta) \quad (6)$$

where σ_x , σ_y , and τ_{xy} are the stress components measured from the measure circles (Itasca 19; Duan and Kwok 9). Figure 2B compares the measured stress components acquired through circular measurements with the theoretical solution of the stress field around the borehole (Eqs. 1, 2 and 3) & (4, 5 and 6). The results reveal that $\sigma_{r\theta}$ exhibits the highest level of agreement, whereas $\sigma_{\theta\theta}$ and σ_{rr} show minor discrepancies. These deviations indicate the existence of high stress concentrations at certain points owing to the geometric heterogeneity resulting from non-uniform-sized particle packing. Since the DEM-based PFC model utilizes the commonly accepted approach of establishing maximum and minimum particle sizes (Song 35; Song et al 31; Bai and Konietzky 3), subtle local stress concentration phenomena are deemed unavoidable.

To ensure that discrete element numerical simulation methods are appropriate for modeling the damage behavior of geo-material, we calibrate the model in both quantitative and qualitative aspects. The reasonability of a numerical model can be evaluated based on two factors: (1) the model

should demonstrate a diverse range of complex macro–micro behaviours similar to those observed in real materials, and (2) the model should replicate damage and failure mechanisms comparable to those of actual materials (Song et al 32).

After carefully comparing the theoretical, experimental, and numerical results, we qualitatively compared the observed macroscopic phenomena during borehole breakout. Figure 3 displays the macroscopic failure mechanisms observed during borehole breakout, which are dominated by tensile spalling resulting from the continuous spalling of broken rock materials or flakes into the borehole, leading to V-shaped breakouts. This occurs due to the extensile microcracks and their coalescence (Fig. 3A, B). Figure 3C displays a selected borehole geometry from a series of simulations in the final stage, demonstrating that the numerical model can accurately reproduce V-shaped fractures and flaky rock peeling. Ultimately, this study provides reasonable confirmation of the numerical model's reliability.

2.3 Simulation Scheme

Many prior studies have demonstrated the ability of discrete element-based numerical simulation methods to more accurately model borehole breakout phenomena (Lin et al 23; Wang et al 36). Depending on the testing design, these experiments can be classified into pre-drilling and pre-stressed tests (Table 2). The pre-drilled loading method significantly reduces the strength of the sample before applying stress, which negatively interferes with the study of borehole fracture behaviour. The pre-stressed loading method is more representative of real-world conditions. Therefore, we adopted the pre-stressed loading method in this study. The construction of the numerical model is illustrated in Fig. 4, with the length and width of the model set at 2 m, and the borehole radius set at 0.02 m.

To better capture changes in stress, three measurement circles were placed in the σ_h direction with a radius of 1/4 of the borehole radius (Fig. 4). The PFC software's built-in fish language measurement circle module was used to extract the stress tensor in each direction and record the corresponding maximum and minimum principal stresses (Itasca 19; Inc, Itasca Consulting Group 19):

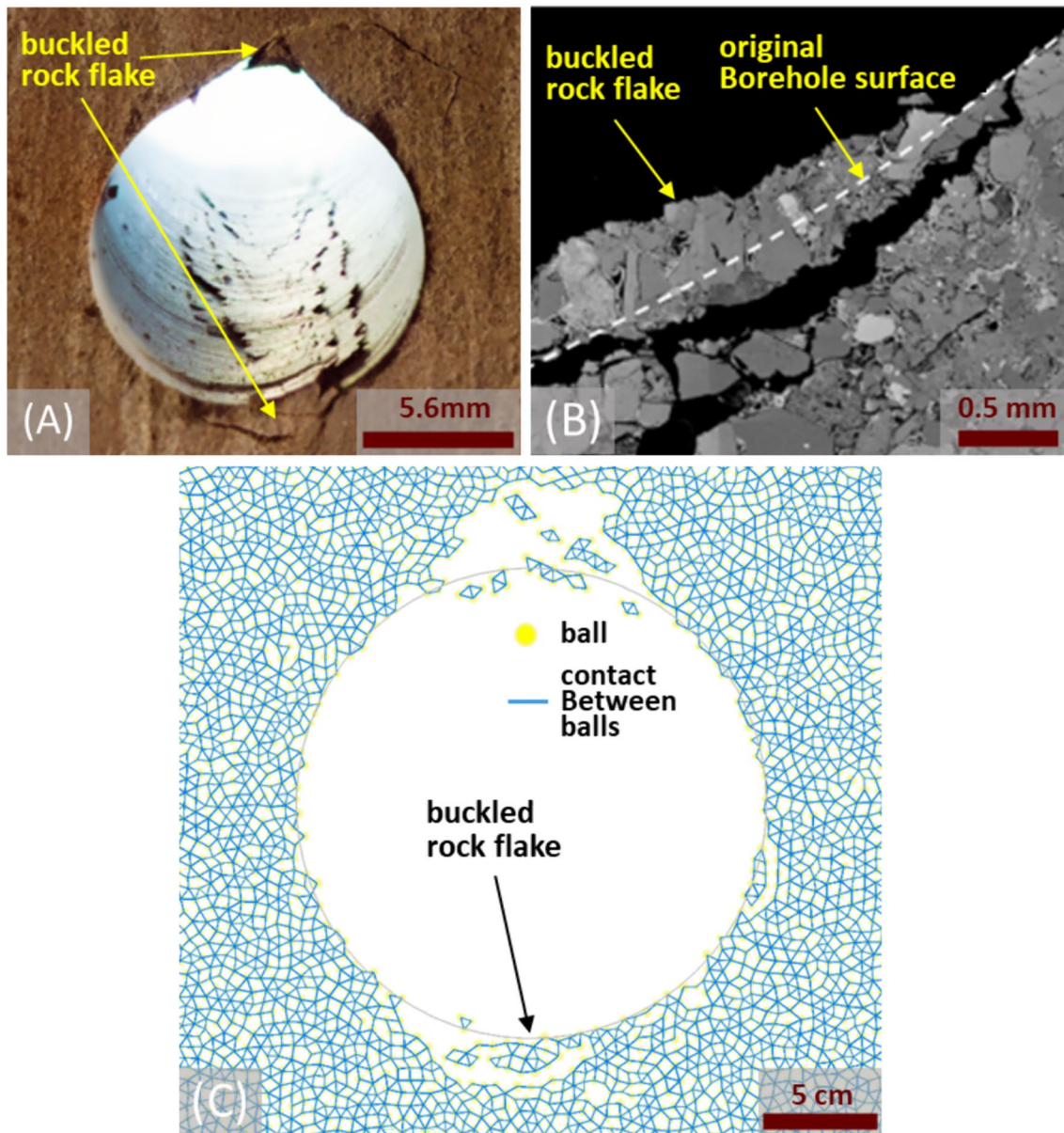


Fig. 3 **A**, Mancos Shale sample PERP 1.2 after deformation, showing V-shaped fracture distribution along the axis of the wellbore (Choens et al 6). **B**, Partial view of the wall of a 1 m vertical borehole in the Lac du Bonnet granite at the Manitoba, showing buckled rock flakes

along a line coinciding with the σ_h springline (Lee et al 21). **C**, closeup of selected timestep in a random case showing V-shape breakout and rock flakes

Table 2 A brief summary of the numerical simulation of borehole breakout under different loading conditions

References	Calibrated via	Loading scheme	Features
Lin (Lin et al 2020)	Sandstone	Pre-drilled	Could undergo macro-scale failure prior to the full development of the breakout
Duan (Duan and Kwok 2016; Duan et al 2018)	Shale	Pre-drilled	
Zhang (Zhang et al 2019)	Gypsum	Pre-drilled	State before drilling is closer to the real geological condition
Xiang (Xiang et al 2023)	Sandstone	Pre-drilled and pre-stressed	
Lee (Lee et al 2016)	Sandstone	Pre-stressed	

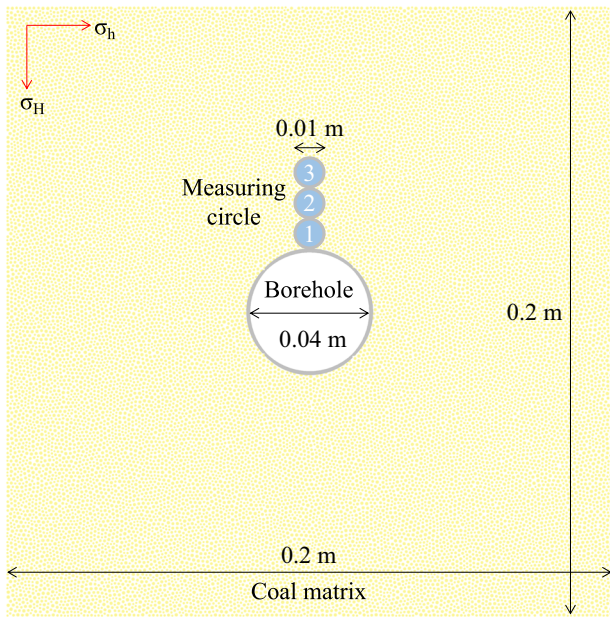


Fig. 4 Model set-up illustrating arrangements of boreholes and measuring circle used for subsequent simulations

Table 3 Sensitivity analysis considering different parameters

Case	Far-field stress σ_H, σ_h (MPa)	Borehole radius (mm)	Young's modulus of coal matrix (GPa)
1	30, 7	20	1.99
2	30, 9	20	1.99
3	30, 12	20	1.99
4	30, 15	20	1.99
5	30, 20	20	1.99
6	30, 25	20	1.99
7	30, 30	20	1.99
8–12	30, 7	18–22	1.99
13–17	30, 9	18–22	1.99
18–22	30, 12	18–22	1.99
23–27	30, 15	18–22	1.99
28–32	30, 20	18–22	1.99
33–37	30, 25	18–22	1.99
38–42	30, 30	18–22	1.99
43	30, 15	20	0.99
44	30, 15	20	2.98
45	30, 15	20	4.10

$$\sigma_{max} = \frac{\sigma_{xx} + \sigma_{yy}}{2} + \sqrt{\left(\frac{\sigma_{xx} - \sigma_{yy}}{2}\right)^2 + \sigma_{xy}^2} \tag{7}$$

$$\sigma_{min} = \frac{\sigma_{xx} + \sigma_{yy}}{2} - \sqrt{\left(\frac{\sigma_{xx} - \sigma_{yy}}{2}\right)^2 + \sigma_{xy}^2} \tag{8}$$

where $\sigma_{xx}, \sigma_{yy}, \sigma_{xy}$ are the stress components recorded from the measuring circles. Before borehole drilling, the model is pre-stressed by applying acceleration to each of the four walls. The velocity applied to the wall at each time increment can be calculated using the following formula:

$$v_w = \frac{\gamma A_w}{k_{mw} N_c \Delta t} |\Delta \sigma| \tag{9}$$

where γ is the relaxation factor, A_w is the area of the wall, k_{mw} is the average stiffness of the contacts on the wall, N_c is the number of contacts acting on the wall, Δt is the corresponding timestep, $\Delta \sigma$ is the difference between the stress required and the current stress of the wall (Itasca 19; Lu et al 24). This technique ensures that the stress values in all directions applied to the sample remain constant throughout subsequent simulation processes. Once the expected confining pressure of the model is attained, borehole drilling behaviour is simulated by removing small spherical particles within the range of the borehole radius. To explicitly study the influence of various factors on the borehole breakout geometry and induced fracture propagation pattern, 45 experimental groups with distinct variables are established (Table 3).

3 Simulation Results and Analysis

In this section, we initially present the progressive damage characteristics of the borehole wall under a specific condition. Subsequently, we conduct simulation calculations in strict accordance with the strategy outlined in Table 3. These calculations aim to investigate the fracture mechanism and geometry around the borehole wall of the coal rock under varying conditions, including far-field stress, borehole radius, young's modulus of the coal seam.

3.1 Progressive Breakout Evolution

For example, case#3 depicts the progressive breakout process shown in Fig. 6. The model is saved and recorded every 2500 timesteps, with the corresponding stress state depicted in Fig. 6. After excavation, stress is redistributed around the borehole, with the upper and lower parts experiencing almost simultaneous damage. The significant stress difference regionally leads to stress concentration at the top and bottom edges of the borehole, and cracks rapidly propagate within 3000 steps (Fig. 6a). At this point, stresses within all measurement circles quickly rise. As cracks continue to propagate rapidly, the maximum principal stress (σ_1) within measurement circle one near the borehole quickly reaches its peak and then rapidly declines. At the same time, higher compressive stress concentrations continue to propagate further into the coal matrix, leading to continuous stress increases within circles 2 and 3.

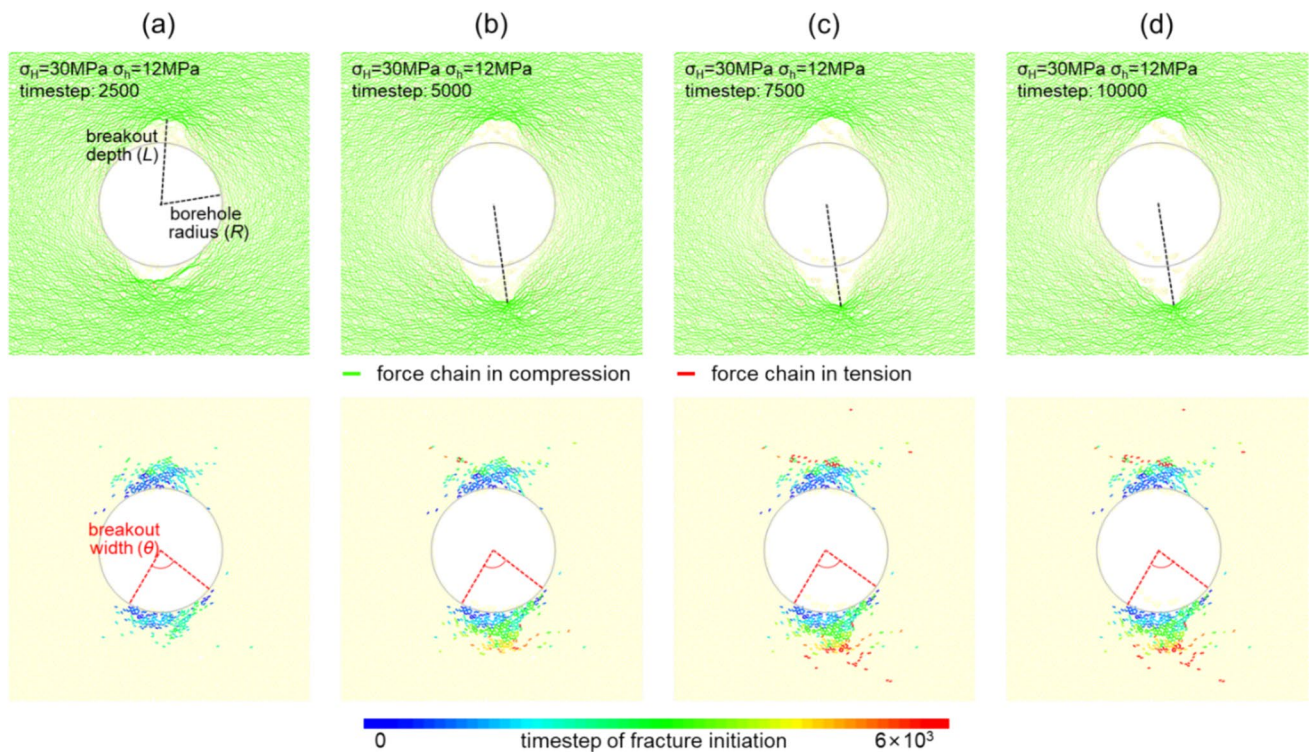


Fig. 5 Progressive failure procedure of borehole breakout of case #3

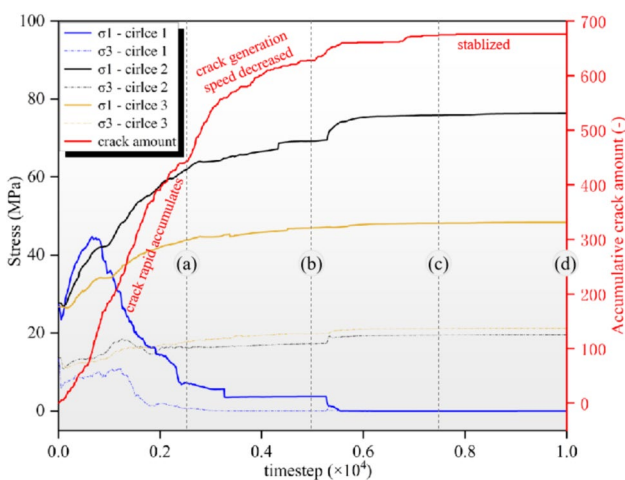


Fig. 6 Principle stress and accumulative crack amount as a function of model timestep

Subsequently, the upper end of the borehole stabilizes and cracks no longer significantly increase in number, while cracks continue to propagate at the lower end of the borehole. This is evidenced by Fig. 5b, which shows the timestep of fracture initiation. By the time the model reaches 7500 steps, cracks are no longer significantly increasing, and only a few new cracks are occurring at the lower edge of the borehole (Fig. 5b). The model stabilizes at around 8000 steps,

with no new cracks and no further stress changes around the borehole (Fig. 6).

The terminal geometry of borehole breakout phenomena in this section is consistent with previous experimental studies, which showed the characteristic “dog-ear” shape along the direction of least resistance. This finding is highly comparable with previous research (Zoback et al 40; Haimson 13; Lee et al 21). To better quantify and compare results, the subsequent analysis focused on normalized depth (L/R) and breakout width (θ) depending on the terminal breakout geometry, allowing for quantitative analysis of the effects of different in-situ stresses, borehole diameters, and coal intrinsic properties in the coal seam (Lin et al 23; Qi et al 27; Xiang et al 37). The black and red dashed lines in Fig. 5 correspond to the normalized depth and breakout width, respectively. Normalized depth represents the ratio of the distance L from the top of the borehole breakout to the borehole centre to the borehole radius R . Breakout width (θ) represents the maximum angle formed by the cracks in contact with the borehole wall and the borehole centre during the breakout. However, in the simulation of coal rock, breakout in both directions of the borehole appears to be symmetric. For ease of analysis, normalized depth and breakout width are always taken as their maximum values (if there are two or more significant breakouts in the current case). Additionally, the volume loss of buckled rock is investigated during

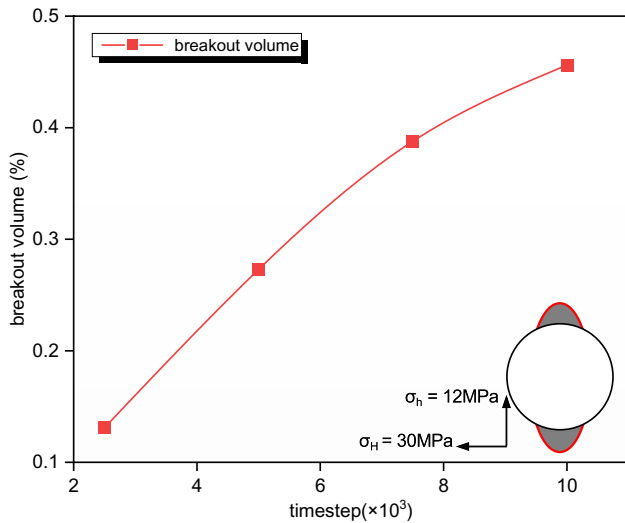


Fig. 7 Evolution of breakout volume

borehole breakout. The following equation represents the breakout volume:

$$R_v = N_d / N_{sum} \tag{10}$$

where N_d is the number of particles detached from the matrix subjected to borehole breakout, which is updated automatically every 2500 timesteps; N_{sum} is the total ball amount at the beginning of the simulation. Figure 7 depicts the evolution of the volume damage rate during the borehole breakout process. As stress redistributes, cracks gradually propagate around the borehole. The volume damage rate (R_v) steadily increases until around 6000 steps, gradually slowing down until the borehole stabilizes.

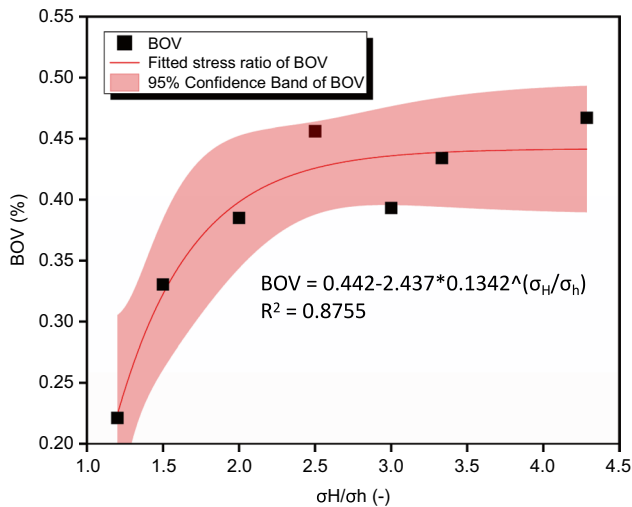


Fig. 8 BOV considering different in-situ stress ratio

3.2 Analysis of Impact Factors

3.2.1 Influence of in-situ Stress

The in-situ stress is a crucial factor in determining borehole breakout geometry. This section conducts a series of simulations (cases 1–7) to reveal the evolution of R_v and breakout geometry under different stress conditions. The stress extracted from the prefabricated measuring circle and accumulative crack amount as a relationship of timestep from selected typical cases are also illustrated. As depicted in Fig. 8, the relationship between stress differences can be expressed using a power function (fitting coefficient $r^2 = 0.8755$). The reason for this pattern is that when the far-field stress difference is large, stress concentration is more likely to occur inside the specimen, inducing more microfractures. This is because a sufficiently large stress difference causes local stress to exceed the tensile/shear strength between adjacent borehole balls, rapidly generating cracks after borehole drilling. However, as the fitting curve shows, the R_v value reaches its maximum when the stress difference is between 2.5 and 3.0 and no longer increases significantly. Consequently, this corresponds to an increase in the total number of accumulated cracks. As the stress difference increases, the R_v value increases according to the power function law and eventually stabilizes. Moreover, the results show that a higher stress difference (greater than 2.5) does not seem to significantly increase the rate of crack generation, as each model runs for 10,000 steps.

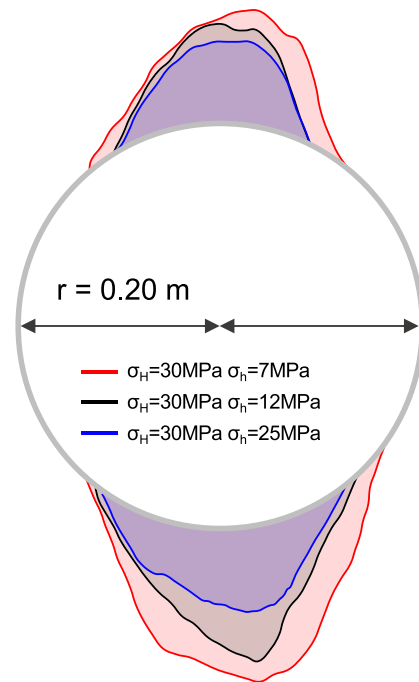


Fig. 9 Terminal breakout geometry under various stress conditions

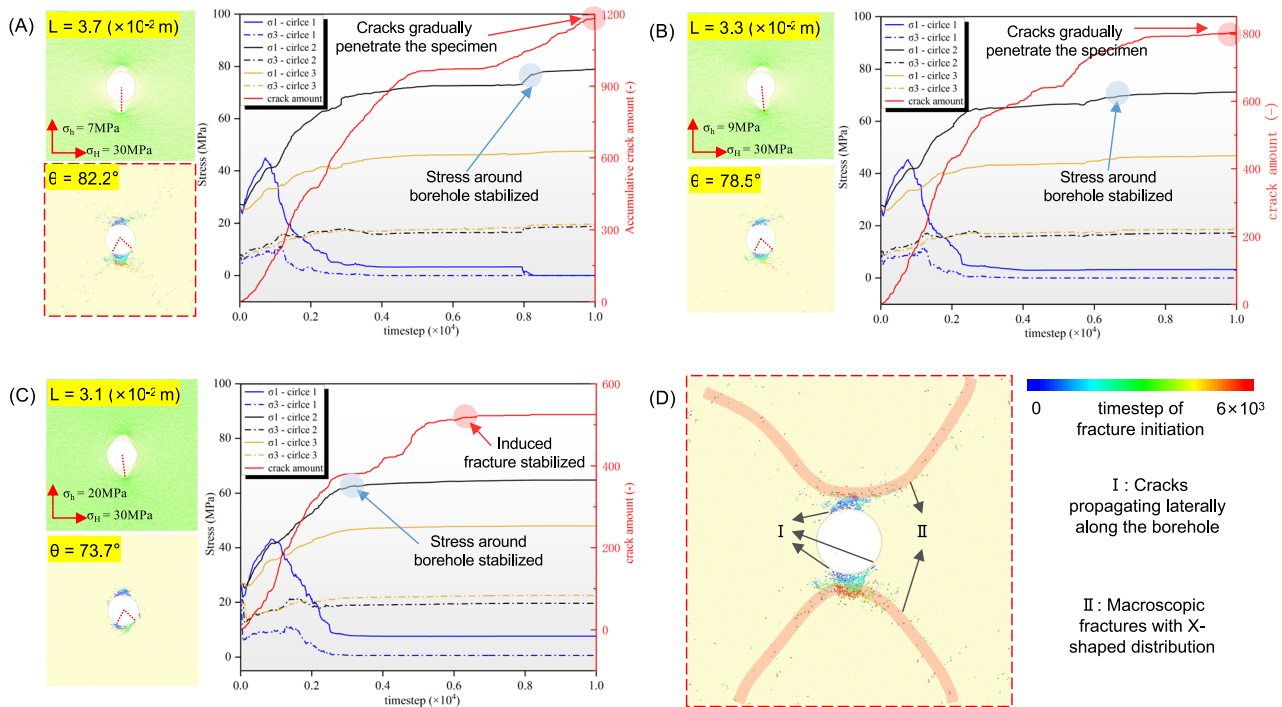


Fig. 10 Terminal geometry and stress evolution of selected cases

In-situ stress not only affects the breakout volume but also significantly alters the breakout geometry. Figure 9 shows the final geometric configuration of the wellbore failures for the selected three cases (case #1, case #3, and case #6). It can be observed that the wellbores in each case fail in the direction perpendicular to the maximum principal stress (in the vertical direction of the wellbore). As the stress difference increases, the width and depth of the V-shaped failure increase, leading to a greater Rv value and an increased number of accumulated cracks.

Figure 10 displays the evolution of stress and accumulated crack number for each case with three measurement circles arranged over time steps. On the left-hand side of each graph, a force chain distribution map is shown, with the thickness of the line indicating the magnitude of the absolute value. This map helps to qualitatively observe stress concentration to determine the farthest crack from the wellbore for fracture depth L . Below the force chains contour is a crack distribution map based on the crack initiation time step. The scale of this map is the same as Fig. 5. After borehole formation, stress quickly concentrates on the borehole due to pre-loading. For instance, in Fig. 10, σ_1 measured from circle #1 initially increases rapidly and then abruptly drops, indicating that the crack zone has gradually passed through circle #1. Between 3000 and 8000 timesteps, the stress measured at both ends of the borehole enters a “stress stable period.” However, during this period, the model’s cracks still increased

rapidly, followed by a tendency to stabilize and then a sharp increase around 7000 time steps. This is because after the coal on both ends of the borehole perpendicular to the maximum principal stress direction (σ_h) is completely damaged, cracks that the measurement circle has not captured continue to occur. These cracks can be classified into two types: (I) transversely extending cracks along the borehole wall. Crack initiation time serves as evidence (Fig. 10D), and this type of crack is observed to accumulate dramatically between 3000 and 4500 time steps (Fig. 10A). (II) Macroscopic conjugate X-shaped cracks. This type of crack is particularly evident when there is a large difference in the applied stress. The macroscopic channelling of this crack implies the final failure of the specimen. As shown in Fig. 11A, after the “stress stable period” (blue dot), the three measurement circles no longer fluctuate in all principal stresses. However, type II cracks increase rapidly until the specimen produces macroscopic X-shaped failure. When the stress difference is 21 MPa (Fig. 10B), the specimen eventually fails due to the gradual increase in type II cracks. However, at this point, the three measurement circles’ maximum and minimum principal stresses have already reached equilibrium much earlier (around 6500 timesteps), indicating that the borehole failure behaviour was completed earlier. When the stress difference is 10 MPa (Fig. 10C), the specimen no longer fails due to the borehole fracture. The stress inside the measurement circle reaches an equilibrium state

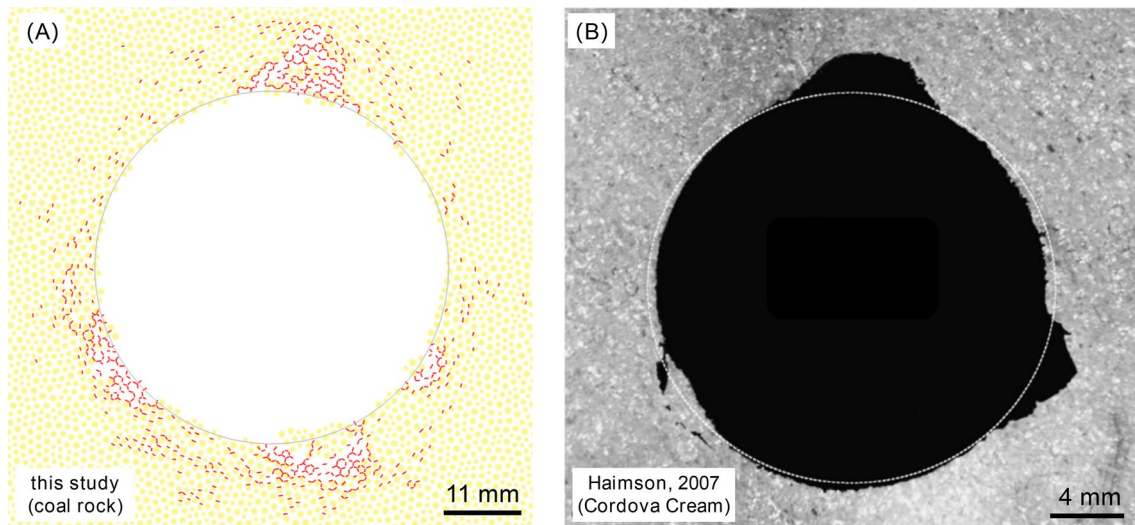


Fig. 11 **A**, simulation result from case # 40 showing 3 breakouts roughly forming an angle of 120 degrees; **B**, Cross-sections of boreholes drilled in Cordova cream under uniform principal horizontal far-field stresses (Haimson 13)

much earlier (around 3000 timesteps). In contrast to the other two cases, type II fractures are no longer generated. Type I cracks continue to occur after the radial fracture is completed (3000–6000 time steps) until the specimen reaches equilibrium.

As evidenced by the force chain patterns in each case, the stress concentration effects towards the ends of the aperture gradually decrease as the stress difference diminishes, and the distribution of force chains around the aperture becomes homogeneous. When the stress difference is zero (under uniform principal horizontal far-field stresses), this stress concentration effect is no longer evident, and directional preference of borehole breakout is absent. Instead of two breakouts aligned with the σ_h springline, three breakouts form around the circumference of the borehole approximately 120 degrees apart. This phenomenon is particularly pronounced in case #40 ($\sigma_H = \sigma_h = 30$ MPa) as depicted in Fig. 11A. This finding corroborates with that of Haimson (Haimson 13), who observed similar results when drilling experiments using Cordova cream under the condition of $\sigma_H = \sigma_h = 40$ MPa.

3.2.2 Borehole Size Effect

The effect of borehole size on breakout geometry was investigated by simulations using five groups of parameters with varying borehole diameters (18, 19, 20, 21, and 22 mm, respectively). Figure 12 demonstrates the evolution of normalized breakout depth, breakout width, and R_v with respect to stress difference for each borehole diameter. It is evident from the figure that borehole size has a significant influence on these three parameters. Figure 12A shows that in most stress conditions, smaller borehole diameters result in larger

normalized breakout depths. Borehole size not only affects the magnitude of normalized breakout depth but also has a considerable impact on its sensitivity to stress conditions. When the borehole diameter is reduced from 21 to 20 mm, the slope of the linear convergence function increases significantly. Figure 12B presents the well-fitted relationship between R_v and stress difference for different borehole diameters, showing that smaller borehole diameters result in larger breakout widths. The linear regression functions for the four borehole diameters reveal that borehole size has a minimal impact on the sensitivity of breakout width to stress conditions. Lastly, as depicted in Fig. 12, R_v exhibits a well-fitted power function relationship with stress difference. However, the influence of borehole size on R_v under different stress conditions does not follow a clear pattern.

3.2.3 Coal Rock's Intrinsic Properties

The geometry of borehole breakout in coal seams is mainly affected by the characteristics of the coal-rock mass. This section presents a numerical simulation study of borehole breakout in coal rocks based on different elastic moduli. In addition to the baseline simulations, three additional sets of simulations were conducted, where the elastic modulus of each numerical model was adjusted to 1–4 GPa while maintaining strength constant (case #4, case #43, case #44, case #45, respectively). An additional parameter calibration was performed for the three coal rocks with different elastic moduli, and the resulting parameters and errors are shown in Table 4.

Figure 13 reveals the variations of the measured in-circle stresses and the accumulated number of cracks over time for the four numerical simulations. The results show that

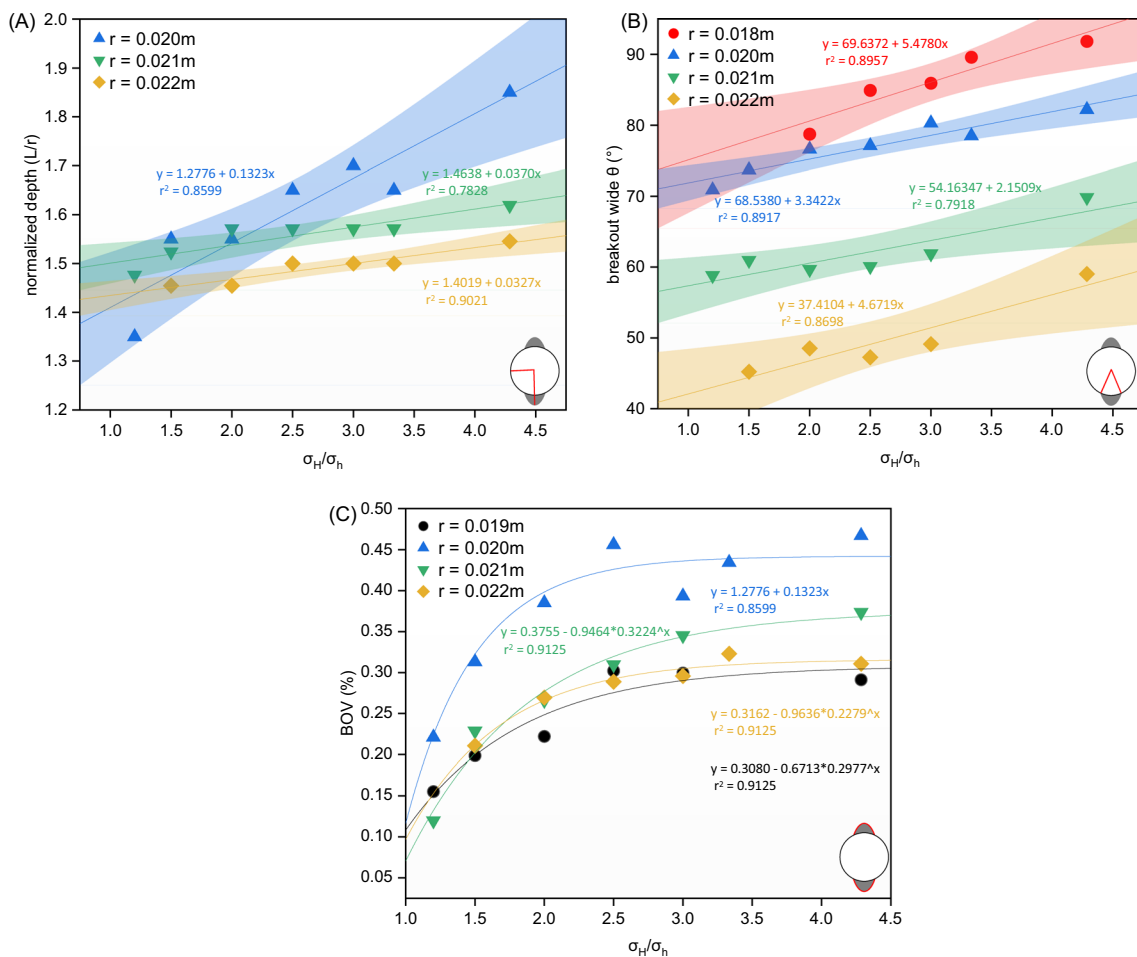


Fig. 12 Normalized depth (L/r) **A**, breakout wide θ ($^\circ$) **B**, and breakout volume (BOV) **C** as a function of stress difference under constant σ_H

Table 4 Input parameters for coal rocks with different Elastic modulus under constant UCS

	I	II	III	IV
Target value for Elastic Modulus (GPa)	1.00	2.00	3.00	4.00
Simulation result for Elastic Modulus (GPa)	0.99	1.99	2.98	4.10
Error (%)	1.00	0.50	0.67	2.55
Target value for UCS (MPa)	26.95	26.95	26.95	26.95
Simulation result for UCS (MPa)	26.28	26.95	26.12	26.12
Error (%)	2.45	0.00	3.08	3.08

with an elastic modulus of 1 GPa, there is no stabilizing period for the measured stresses and accumulated cracks in the three measuring circles. After 10,000 time steps, the stresses in measuring circles #1 and #2 have decreased to zero, indicating that the breakout tip has passed through the

range of circles #1 and #2, releasing the stress sufficiently. The number of cracks increases significantly until a macroscopic X-shaped damage appears, causing the specimen to fracture. For an elastic modulus of 2 GPa, type I cracks appear around the 3000th time step (blue-shaded area), and the drilling-induced breakout is completed around the 6600th step, reaching a balanced state (red-shaded area). Type I cracks begin to emerge later at around the 6700th time step for an elastic modulus of 3 GPa. For an elastic modulus of 4 GPa, the specimen reaches a stable state at the earliest (around the 4150th step).

Figure 14 presents normalized breakout depth, breakout width, and Rv as a function of elastic modulus. As the elastic modulus increases, normalized depth shows a clear monotonic decrease when the stress difference is assigned as 21 and 18 MPa (Fig. 14A). When the stress difference is assigned as 15 and 18 MPa, the breakout width decreases monotonically with the increasing elastic modulus (Fig. 14B). Rv shows a clear monotonic decrease for 15 and 21 MPa stress differences. These three figures

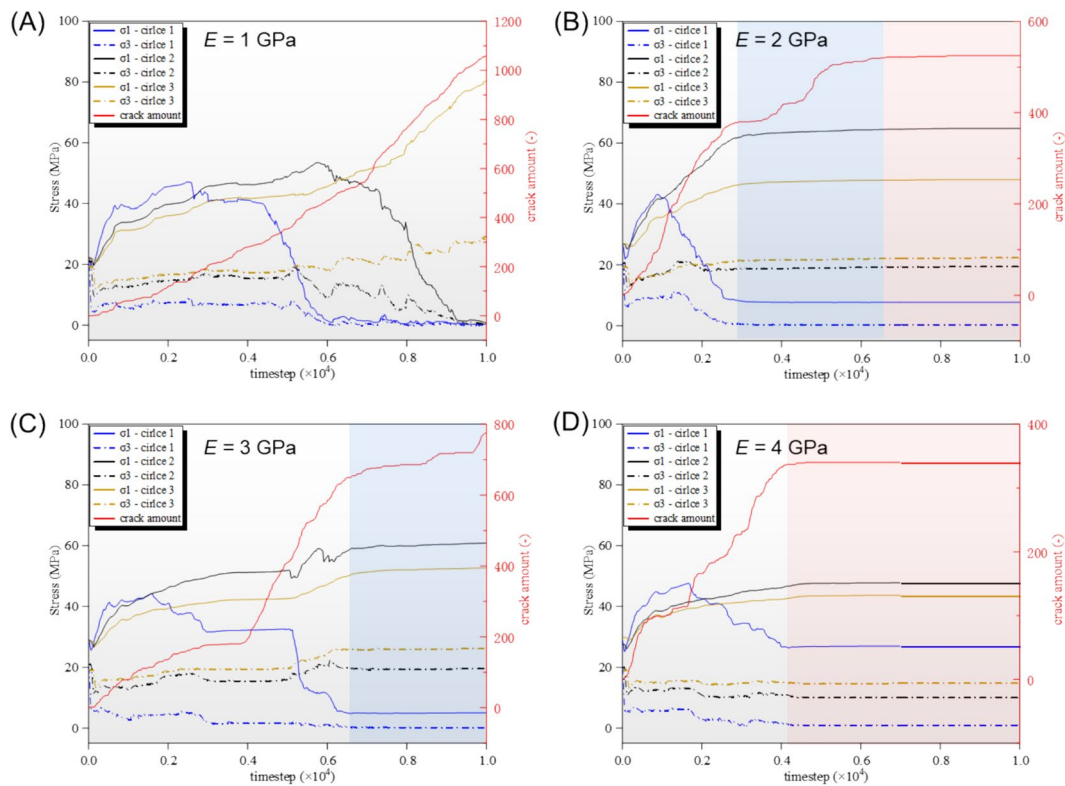


Fig. 13 Evolutions of stress and accumulative crack amount for different Young's modulus: **A**, 2 GPa; **B**, 2 GPa; **C**, 3 GPa; **D**, 4 GPa

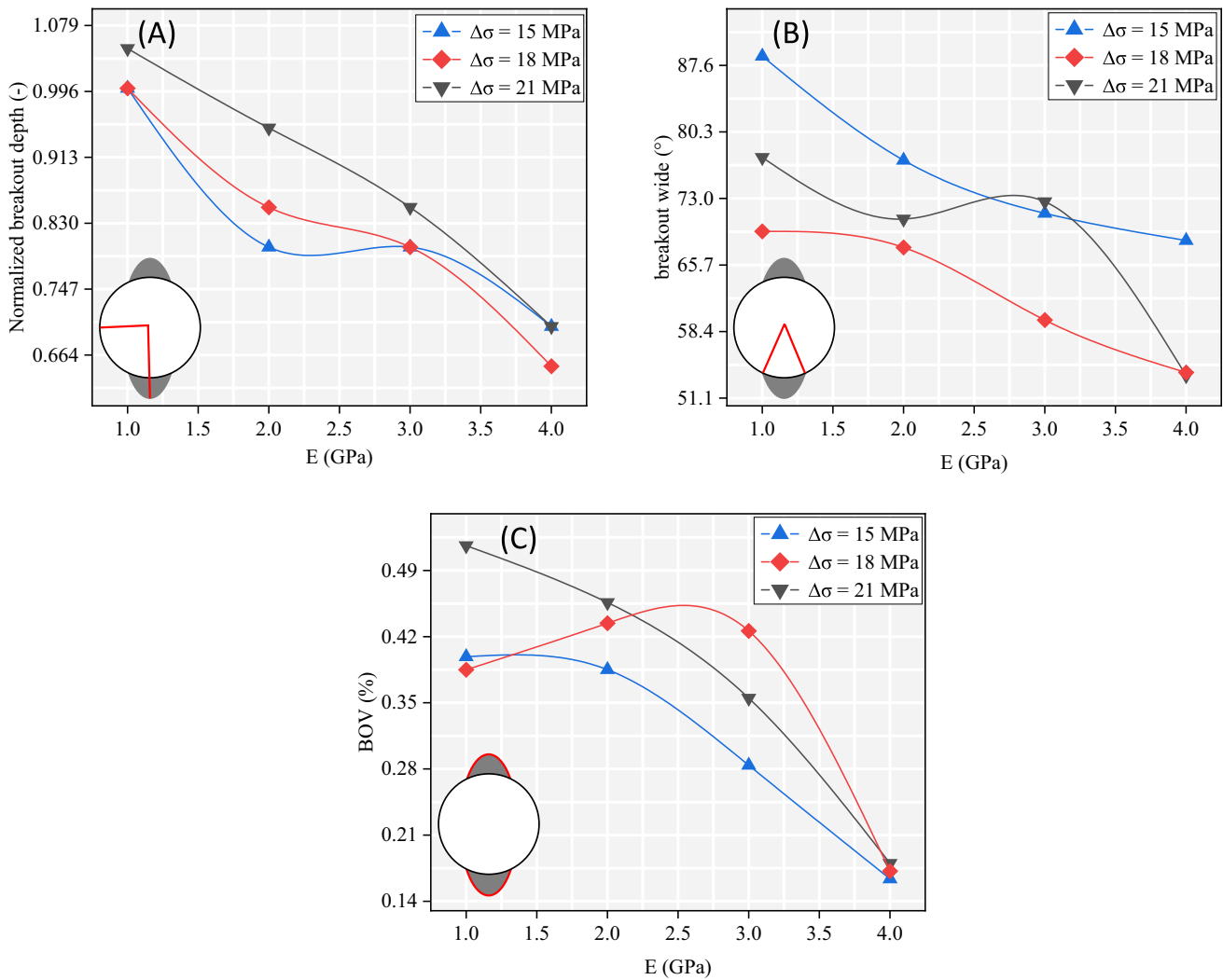
indicate that an increase in elastic modulus significantly inhibits the borehole breakout geometry in coal rocks.

4 Discussion

The influence of coal elastic modulus on breakout geometry can be explained as follows: (1) After the development of a free surface/space due to drilling, stress concentration occurs at both ends perpendicular to the maximum principal stress (in this paper represented by σ_H as the X direction and stress concentration occurring at the two ends of the Y direction). Micro fractures initiate when regional tensile stress induced by stress concentration exceeds the bond strength between discrete ball elements. (2) The micro fractures form and coalesce at the bore wall, and as the fractures continue to generate, the fracture tip forms and extends along the minimum in-situ stress direction. (3) When the fracture tip stops extending, the crack expands laterally along the bore wall. In some cases, X-shaped conjugate cracks can occur until macroscopic failure. As previously discussed, the distribution of I and II-typed cracks occurs. Geo stress is an essential factor affecting unstable cracks in bore walls. As the stress difference decreases, the stress concentration effect along the minimum principal stress direction weakens, and

the initiation and accumulation of cracks are suppressed. At this point, the distribution pattern of crack inclination changes from “concentrated at both ends at about 0 and 180 degrees” to “roughly uniformly distributed.” (Fig. 15). Therefore, breakout geometry changes from “symmetrical development at both ends” to “uniform distribution at an angle close to 60 degrees.” Overall, the mechanism of coal elastic modulus influencing breakout geometry is complex and involves several factors that must be considered.

Qualitatively speaking, the borehole instability pattern based on coal rock is consistent with the experimental results reported in previous literature based on other rocks (see Fig. 11). However, a quantitative comparison of the borehole instability geometry in coal seams with the data obtained based on other rock types in previous literature reveals significant differences. Coal rock breakout width is not very sensitive to stress difference and remains relatively high, mostly between 70 and 80° (Fig. 16A). Similarly, normalized breakout depth in coal rock exhibits initial high values and low fluctuations compared to sandstone (Fig. 16B). Overall, these observations show that the mechanism of borehole instability in coal rock is unique and must be carefully considered when studying rock mechanics and drilling engineering.



(Li et al. 2019)

Fig. 14 Normalized depth **A**, breakout wide **B** and breakout volume **C** as a function of stress difference under constant σ_H (Li et al 22)

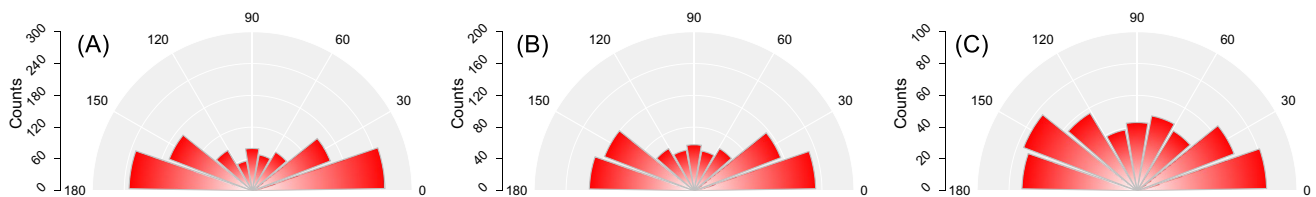


Fig. 15 Terminal microcrack distribution pattern considering different stress difference, each of the three scenarios corresponds to that in Fig. 10, respectively

Furthermore, the simulation results of coal rock with different elastic moduli in the previous section showed that not all models remain stable after borehole fracturing when the elastic modulus changes. In addition to the cases introduced at the beginning of Sect. 2.3, this section performed

simulations with different stress differences for each elastic modulus until the sample was stable or destroyed. It is crucial to consider the variations in elastic modulus and stress difference when studying borehole instability in coal rock.

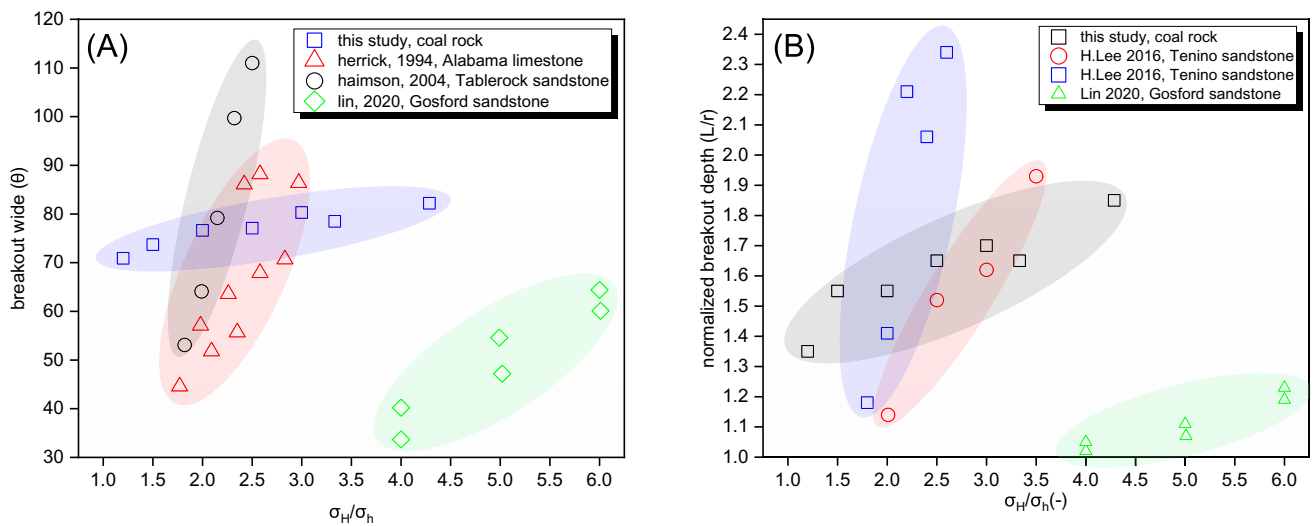


Fig. 16 Normalized breakout length **A** and width **B** in relation to stress difference: a brief comparison of those in coal and other rock masses

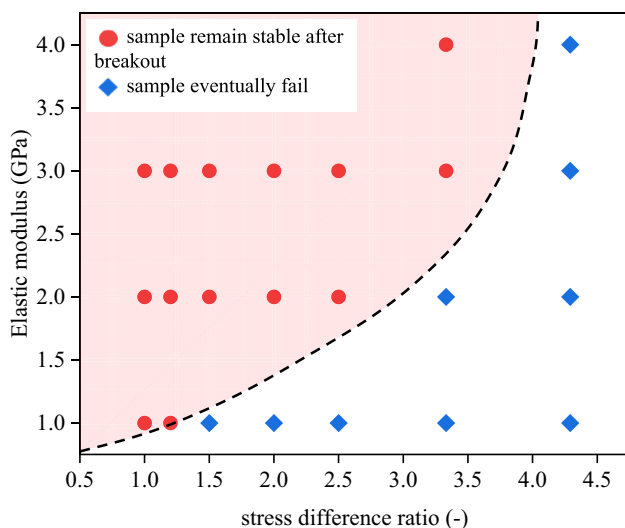


Fig. 17 Critical line between stable tendency and failure tendency considering stress difference and elastic modulus

It was discovered that there is a critical line at which coal samples ultimately fracture due to the impact of borehole instability (Fig. 17). When the elastic modulus of coal rock is presented as a variable of stress difference, the critical line generally shows a power function relationship. The smaller the stress difference, the larger the safe range (the red-shaded area), and the stronger the tendency for stability after coal seam drilling breakout. As the stress difference increases, there is a stronger tendency for macroscopic fracture after the coal seam drilling breakout, and the hardness of the coal seam has less control over the eventual occurrence of macroscopic cracks. In other words, when the stress difference is more prominent, borehole instability may ignore the elastic modulus of the coal seam, ultimately resulting in

macroscopic cracks. This observation provides theoretical references for engineering applications in coal mines.

5 Conclusion

We implement a DEM-based model using PFC 5.0-2D software to comprehensively investigate borehole breakout in coal rock, revealing the influence of in-situ geo stress, borehole diameter, and coal intrinsic properties on the breakout geometry under pre-stressed conditions. We found that the breakout geometry in coal rock is highly sensitive to stress differences. Breakout depth and width show a linear positive correlation with stress differences, with linear convergence coefficients ranging from 0.78 to 0.90 under different borehole sizes, while R_v shows an exponential function correlation with stress differences. As stress differences increase, the R_v value first increases and then stabilizes. The convergence coefficients under different borehole sizes range from 0.86 to 0.91. Furthermore, parameters used to describe borehole breakout geometry (breakout depth, breakout wide) in coal seams show similar characteristics to sandstone but with initially high values and low fluctuations as the stress difference changes. In other words, borehole instability in coal seams is apparent once it occurs. However, compared to sandstone and limestone, breakout depth and width in coal seams show lower sensitivity to the in-situ stress. Finally, an increased elastic modulus has a significant inhibitory effect on breakout geometry under various stress differences. The smaller the elastic modulus, the more prone the coal body is to macroscopic damage after borehole instability. A critical line for borehole breakout in coal rock is proposed based on the combined influence of the

elastic modulus and stress difference, where the area below the critical line represents the tendency for macroscopic damage after borehole instability, and the area above represents the tendency to remain stable. These results offer valuable insights into engineering sites and contribute to advancing knowledge of borehole breakout in coal rock.

Author's contribution *Huang Shan* Conceptualization, Methodology, Writing—Original Draft; *Lu Yiyu* Supervision, Funding acquisition; *Ge Zhaolong* Methodology, Software, Validation; *Yunzhong Jia* Validation, Formal analysis, Investigation; *Zhou Zhe* Resources, Data Curation; *Lu Changzheng* Writing—Review & Editing, Visualization.

Funding No funding was received for conducting this study

Data availability Not applicable.

Declarations

Conflict of interest The authors declare that they have no conflict of interest.

References

- Ai C, Hu C, Zhang Y, et al (2014) Wellbore stability estimation model of horizontal well in cleat-featured coal seam. *Soc Pet Eng - Eur Unconv Resour Conf Exhib 2014 Unlocking Eur Potential*, 2:787–795. <https://doi.org/10.2118/167767-ms>
- Bai Q, Konietzky H, Dang W (2022) Microscopic modeling of frictional response of smooth joint under normal cyclic loading. *Rock Mech Rock Eng* 55:169–186. <https://doi.org/10.1007/s00603-021-02652-3>
- Bai Q, Konietzky H (2022) Numerical insight into energy partitioning during stick-slip events based on the framework of rate-and-state friction law. *Geophys Res Lett*. <https://doi.org/10.1029/2021GL096677>
- Barton CA, Zoback MD, Burns KL (1988) In-situ stress orientation and magnitude at the Fenton Geothermal Site. *Geophys Res Lett* 15:467–470
- Cheatham JB (1993) A new hypothesis to explain stability of borehole breakouts. *Int J Rock Mech Min Sci* 30:1095–1101. [https://doi.org/10.1016/0148-9062\(93\)90077-Q](https://doi.org/10.1016/0148-9062(93)90077-Q)
- Choens RC, Lee MY, Ingraham MD et al (2019) Experimental studies of anisotropy on borehole breakouts in mancos shale. *J Geophys Res Solid Earth* 124:4119–4141. <https://doi.org/10.1029/2018JB017090>
- Cundall PA (1971) A computer model for simulating progressive, large-scale movements in blocky rock systems. *Proc Int Symp Rock Fract*
- Duan K, Wu W, Kwok CY, Yee C (2018) Discrete element modelling of stress-induced instability of directional drilling boreholes in anisotropic rock. *Tunn Undergr Sp Technol* 81:55–67. <https://doi.org/10.1016/j.tust.2018.07.001>
- Duan K, Kwok CY (2016) Evolution of stress-induced borehole breakout in inherently anisotropic rock: insights from discrete element modeling. *J Geophys Res Solid Earth*. <https://doi.org/10.1002/2015JB012676>. Received
- Fairhurst C (1968) Methods of determining in-situ rock stresses at great depth. *Tech Rep I-86*, Missouri River Div US Army Corps Eng
- Fakhimi A, Carvalho F, Ishida T, Labuz JF (2002) Simulation of failure around a circular opening in rock. *Int J Rock Mech Min Sci* 39:507–515. [https://doi.org/10.1016/S1365-1609\(02\)00041-2](https://doi.org/10.1016/S1365-1609(02)00041-2)
- Fushan C, Zhonghui L, Yishan L, et al (2015) Research Method of Wellbore Stability of Coal Formation in the Daniudi Gas Field. *CHINA PETROLEUM Mach*
- Haimson B (2007) Micromechanisms of borehole instability leading to breakouts in rocks. *Int J Rock Mech Min Sci* 44:157–173. <https://doi.org/10.1016/j.ijrmms.2006.06.002>
- Haimson B, Lee H (2004) Borehole breakouts and compaction bands in two high-porosity sandstones. *Int J Rock Mech Min Sci* 41:287–301. <https://doi.org/10.1016/j.ijrmms.2003.09.001>
- Hazzard JF, Young RP, Al-Busaidi A et al (2005) Distinct element modeling of hydraulically fractured Lac du Bonnet granite. *J Geophys Res Solid Earth* 110:1–14. <https://doi.org/10.1029/2004JB003297>
- He S, Ou S, Lu Y et al (2022) Failure mechanism of methane drainage borehole in soft coal seams: insights from simulation, theoretical analysis and in-borehole imaging. *Process Saf Environ Prot* 168:410–421. <https://doi.org/10.1016/j.psep.2022.10.012>
- Van den Hoek PJ (2001) Prediction of different types of cavity failure using bifurcation theory. *Proc 38th rock Mech Symp* 45–52
- Inc, Itasca Consulting Group U (2018) PFC 5.0 documentation
- Itasca (2010) PFC2D-Particle Flow Code in two dimensions. Ver. 4.0 User's Manual. ICG, Minneapolis
- Jianping W, Yubo C, Yong L (2024) Progress and trends in non-tool rock breaking theory and technology. *J China Coal Soc* 49:
- Lee H, Moon T, Haimson BC et al (2016) Borehole breakouts induced in Arkosic sandstones and a discrete element analysis. *Rock Mech Rock Eng* 49:1369–1388. <https://doi.org/10.1007/s00603-015-0812-0>
- Li X, El Mohtar CS, Gray KE et al (2019) Modeling progressive breakouts in deviated wellbores. *J Pet Sci Eng* 175:905–918. <https://doi.org/10.1016/j.petrol.2019.01.007>
- Lin H, Kang WH, Oh J et al (2020) Numerical simulation on borehole breakout and borehole size effect using discrete element method. *Int J Min Sci Technol* 30:623–633. <https://doi.org/10.1016/j.ijmst.2020.05.019>
- Lu Y, Huang S, Ge Z et al (2023) Fluid-driven cracking behavior of coal with prefabricated plane : a particle-based hydro-mechanical coupled numerical investigation. *Theor Appl Fract Mech* 124:103825. <https://doi.org/10.1016/j.tafmec.2023.103825>
- Marschall P, Distinguin M, Shao H, et al (2006) Creation and evolution of damage zones around a microtunnel in a claystone formation of the swiss jura mountains. <https://doi.org/10.2118/98537-ms>
- Potyondy DO, Cundall PA (2004) A bonded-particle model for rock. *Int J Rock Mech Min Sci* 41:1329–1364. <https://doi.org/10.1016/j.ijrmms.2004.09.011>
- Qi G, Songcai H, Xian S, et al (2022) Effect of parent well production on wellbore breakout of child well in coalbed methane reservoirs. <https://doi.org/10.56952/arma-2022-0022>
- Ruichen S (2010) Research progress and development trend of coal seam wellbore stability technology. *Pet Drill Tech (in Chinese)*. 10.3969/issn.1001-0890.2010.03.001
- Sokolnikoff IS, Specht RD (1956) *Mathematical theory of elasticity*. McGraw-Hill, New York
- Song Z, Konietzky H, Herbst M (2019) Three-dimensional particle model based numerical simulation on multi-level compressive cyclic loading of concrete. *Constr Build Mater* 225:661–677. <https://doi.org/10.1016/j.conbuildmat.2019.07.260>
- Song Z, Konietzky H, Herbst M (2020) International Journal of Rock Mechanics and Mining Sciences Drawing mechanism of fractured top coal in longwall top coal caving. *Int J Rock Mech Min Sci* 130:104329. <https://doi.org/10.1016/j.ijrmms.2020.104329>

- Song Z, Yang Z, Zhang M et al (2023) Numerical characterization of sandstone's mechanical responses under multi-level compressive differential cyclic loading (DCL): a 3D particle-based numerical investigation. *Comput Geotech* 154:105109. <https://doi.org/10.1016/j.compgeo.2022.105109>
- Song Z, Yang Z, Herbst M, et al Mechanical characterization of sandstone exposed to variable- amplitude compressive differential cyclic loading (DCL): a 3D particle based numerical study
- Song (1998) Borehole breakouts and core diskings in Westerly granite: mechanisms of formation and relationship to in situ stress. University of Wisconsin
- Song Z (2018) Bonded-particle model-based simulation of artificial rock subjected to cyclic loading. *Acta Geotech* 9:.. <https://doi.org/10.1007/s11440-018-0723-9>
- Wang T, Huang H, Zhang F, Han Y (2020) DEM-continuum mechanics coupled modeling of slot-shaped breakout in high-porosity sandstone. *Tunn Undergr Sp Technol* 98:103348. <https://doi.org/10.1016/j.tust.2020.103348>
- Xiang Z, Moon T, Si G et al (2023) Numerical analysis of v-shaped borehole breakout using three-dimensional discrete-element method. *Rock Mech Rock Eng*. <https://doi.org/10.1007/s00603-023-03226-1>
- Xu H, Wang G, Fan C et al (2020) Grain-scale reconstruction and simulation of coal mechanical deformation and failure behaviors using combined SEM Digital Rock data and DEM simulator. *Powder Technol* 360:1305–1320. <https://doi.org/10.1016/j.powtec.2019.07.014>
- Zhang S, Li Y, Shen B et al (2019) Effective evaluation of pressure relief drilling for reducing rock bursts and its application in underground coal mines. *Int J Rock Mech Min Sci* 114:7–16. <https://doi.org/10.1016/j.ijrmms.2018.12.010>
- Zoback MD, Moos D, Mastin L, Anderson RN (1985) Well Bore Breakouts and in Situ Stress. *J Geophys Res* 90:5523–5530. <https://doi.org/10.1029/JB090iB07p05523>

Publisher's Note Springer Nature remains neutral with regard to jurisdictional claims in published maps and institutional affiliations.

Springer Nature or its licensor (e.g. a society or other partner) holds exclusive rights to this article under a publishing agreement with the author(s) or other rightsholder(s); author self-archiving of the accepted manuscript version of this article is solely governed by the terms of such publishing agreement and applicable law.